Experimental Thermochemistry of SiCl$_3$R (R = Cl, H, CH$_3$, C$_2$H$_5$, C$_2$H$_3$, CH$_2$Cl, SiCl$_3$), SiCl$_3$$^+$, and SiCl$_3$$^\bullet$

Nicholas S. Shuman, Austin P. Spencer, and Tomas Baer*

Department of Chemistry, University of North Carolina at Chapel Hill, Chapel Hill, North Carolina 27599-3290

Received: June 9, 2009; Revised Manuscript Received: July 10, 2009

The 0 K onsets (E_0) of a series of trichlorosilane derivatives SiCl$_3$R → SiCl$_3$$^+$+ R$^\bullet$ (R = Cl, H, CH$_3$, C$_2$H$_5$, C$_2$H$_3$, CH$_2$Cl, SiCl$_3$) are measured by threshold photoelectron−photoion coincidence spectroscopy. The well-known heat of formation of SiCl$_4$ is used as an anchor to determine the heat of formation of SiCl$_3$$^+$, which is, in turn, used as an anchor to determine the heats of formation of the other alkyltrichlorosilanes investigated. A series of isodesmic reactions at the G3 and CBS-QB3 levels are shown to accurately reproduce the experimental heats of formation, and this scheme is used to calculate the heat of formation of Si$_2$Cl$_6$, from which the measured E_0 determines the SiCl$_3$$^\bullet$ heat of formation. The measured values then determine the IE of SiCl$_3$$^\bullet$ along with the Si−R bond dissociation enthalpies of the six neutral species investigated. The experimental heats of formation are also used in a series of isodesmic reaction calculations to determine the heats of formation of SiH$_3$R (R = H, CH$_3$, C$_2$H$_5$, C$_2$H$_3$, CH$_2$Cl, SiCl$_3$).
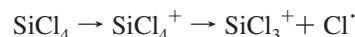
Introduction

Two recent studies[1,2] have reported on the thermochemistry of halogenated silanes through high-level calculations. There is interest in the energetics of these molecules because of their importance in chemical vapor deposition, surface-etching of semiconductor metals, and chemical hydrogen storage systems. The theoretical studies aimed to fill a gap where very little experimental data exist. It is thus of considerable interest to obtain accurate experimental energies that can be compared to the calculated results. In particular, there are large discrepancies between calculated heats of formation and some of the few experimental values which must be addressed.[1]

The lack of experimental data is a result of several factors. Few calorimetry experiments were carried out on these molecules, and those that were, often appear unreliable due to uncertainty in the final state of Si. Thermochemical determinations necessarily depend on measuring the energy difference between reactants and products, thereby connecting an unknown species to ones that are well-established. However, the sparseness of reliable calorimetric data on similar compounds prevented other commonly employed thermochemical methods, such as determining equilibrium constants between two reacting species, from being employed. Finally, in addition to the lack of reliable anchors, bond energies in many alkyl silanes are difficult to determine through photoionization or electron impact because the lowest energy dissociations tend to involve complex rearrangements,[3,4] and the likely presence of reverse barriers prevents determining the threshold energies for dissociation.
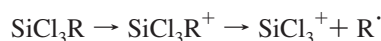
SiCl$_4$ is one of the few silanes with a well-determined heat of formation and, therefore, one of the few reliable anchors for related compounds. The NIST−JANAF compilation reports the 298 K ΔH_f^0 as −662.8 ± 1.3 kJ mol^{-1} based on a pair of calorimetry measurements.[5] Although we agree with the evaluation of Walsh[6] that this uncertainty appears overly optimistic, on the basis of the excellent agreement between the experimental

value and more recent high-level calculations,[1] we reject Walsh's suggestion of an uncertainty of more than 5 kJ mol^{-1} and adopt a value of −662.8 ± 2 kJ mol^{-1} for use in the current study.

The lowest energy dissociation channel of SiCl$_4$$^+$ is

$$SiCl_4 \rightarrow SiCl_4^+ \rightarrow SiCl_3^+ + Cl^\bullet$$

Because the heat of formation of the chlorine radical is, of course, very well-known, accurate measurement of the threshold for this process determines the heat of formation of SiCl$_3$$^+$. Similar to Si(CH$_3$)$_3$$^+$,[7] this is a rather stable ionic species, and the ions of many other compounds that include the SiCl$_3$ subgroup will also dissociate via

$$SiCl_3R \rightarrow SiCl_3R^+ \rightarrow SiCl_3^+ + R^\bullet$$

Assuming the heat of formation of the radical is known, SiCl$_3$$^+$ can be used as an anchor to determine the heat of formation of the neutral species. Additionally, if the ionization energy of SiCl$_3$$^\bullet$ can be determined, then the Si−R bond dissociation enthalpies of the neutral species are also determined.

Here, we use threshold photoelectron−photoion coincidence (TPEPICO) spectroscopy to measure the 0 K onsets (E_0) to dissociation of a series of trichlorosilane derivatives (SiCl$_4$, SiCl$_3$H, SiCl$_3$CH$_3$, SiCl$_3$C$_2$H$_5$, SiCl$_3$C$_2$H$_3$, SiCl$_3$CH$_2$Cl, Si$_2$Cl$_6$). Although these are not the species of the most practical interest (rather, these are species from which reliable thermochemistry may be derived from the experiment), comparison with the experimental thermochemistry allows for evaluation of the accuracy of theoretical methods on these and related molecules. Additionally, the experimental heats of formation of these species can be used in isodesmic reaction calculations of the heats of formation of similar species that are of more interest, significantly improving the accuracy of whatever theoretical method is applied in comparison to calculation of atomization energies.

---

* Corresponding author. E-mail: baer@email.unc.edu.

Thermochemistry of SiCl$_3$R, SiCl$_3^+$, and SiCl$_3^•$

J. Phys. Chem. A, Vol. 113, No. 34, 2009 **9459**

Experimental Methods

The TPEPICO apparatus has been described in detail previously,[8–10] and only a brief description appears here. Sample vapor passes into the ionization region of the high-vacuum chamber through a copper inlet held at a temperature variable between 215 and 400 K. The sample is ionized by vacuum ultraviolet radiation originating from a molecular hydrogen discharge lamp and dispersed by a 1 m normal incidence monochromator providing photon resolution of about 8 meV at 10 eV. A 20 V cm^{-1} gradient (40 V cm^{-1} in the case of SiCl$_3$H) accelerates electrons and ions in opposite directions. Electrons are accelerated by velocity focusing optics such that a Channeltron electron multiplier masked by a 1.4 mm diameter aperture detects only electrons with zero kinetic energy perpendicular to the acceleration axis. A second Channeltron sits off-axis masked by a 2 mm × 6 mm rectangular aperture and collects a portion of the isotropically distributed energetic electrons. The off-axis signal is used to subtract the on-axis signal due to energetic electrons such that the remaining on-axis signal is composed solely of threshold (zero kinetic energy) electron events. The ions collected in coincidence with the threshold electrons are energy-selected in that the ion internal energy is the sum of the incident photon energy and the initial thermal energy of the molecule. Ions pass through a time-of-flight (TOF) mass spectrometer, with "time-zero" indicated by detection of the coincident electron. The mass spectrometer consists of two acceleration regions; a 27 cm, field-free drift region; a deceleration region; and a final 7 cm drift region. The deceleration voltage serves to separate parent ions and ions which dissociate in the first field-free drift region. Each resulting TOF mass spectrum at a given photon energy indicates the dissociation probability of ions with a well-defined distribution of internal energies.

Computational Details

All calculations presented here were carried out with the Gaussian03 quantum chemical software.[11] All vibrational frequencies and rotational constants used in data modeling and thermal energy calculations are those determined from geometries optimized at the B3LYP/6-311++G(d,p) level, and vibrational frequencies are used unscaled.[12] Frequencies used to describe the "transition state" of barrierless dissociations in the Rice–Ramsperger–Kassel–Marcus (RRKM) treatment were estimated by a constrained optimization of the dissociating species with the breaking bond held at approximately 3 Å. The resulting imaginary frequency is confirmed to closely correspond to the reaction coordinate by visualizing the mode using Gaussview software, and the lowest real frequencies are assumed to be the disappearing transitional modes and are treated as optimizable parameters in the analysis. The number of disappearing modes depends on the neutral fragment; namely, two modes for atom loss, four modes for the loss of a diatomic, and five modes for the loss of a nonlinear polyatomic neutral fragment. In dissociations that pass through an energetic maximum, transition states were found using the STQN method at the B3LYP/6-311++G(d,p) level, and the critical mode was confirmed to correspond to the reaction coordinate by visualization of the mode using Gaussview software. Calculated harmonic vibrational frequencies are reported as online Supporting Information. All reported calculated heats of formation are derived from isodesmic reaction calculations using electronic energies evaluated with both the G3[13] and CBS-QB3[14] model chemistries.
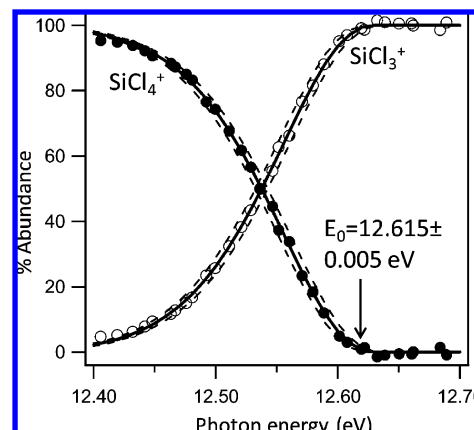

Figure 1. Breakdown diagram of SiCl$_4^+$. Open and closed circles are experimental abundances. Solid lines are the data modeled at the best-fit E_0 as described in the text. Dashed lines are the modeled data at the edges of the uncertainty limits.

Results and Analysis

SiCl$_4$. Several previous studies report the appearance energy of SiCl$_3^+$ from SiCl$_4$ by either electron impact[3,4] or photoionization mass spectrometry.[15] However, extracting accurate thermochemical values from such measurements is problematic for two reasons: First, the appearance energy is typically determined by an extrapolation of the linear portion of the photoionization curve down to zero, and there tends to be ambiguity in which portion of the curve is correctly described as linear. Second, the appearance energy determined is dependent on the temperature of the sample,[16] shifting to lower energies for warmer samples, away from the 0 K value that is true thermochemical threshold. Although a post hoc adjustment based on the average thermal energy of the molecule at the measured temperature can nominally convert an appearance energy to the 0 K value,[16] a much more precise determination of E_0 can be made if the dissociating ions are energy-selected, as is done in a TPEPICO measurement.

The breakdown diagram (the relative abundances of the parent and daughter ions as a function of photon energy) collected for SiCl$_4$ at 230 K is shown in Figure 1. The daughter ion peaks in the TOF spectra for this reaction were symmetric, indicating that the dissociation occurs fast on the time scale of our experiment. That is, any ion with sufficient internal energy to dissociate does so in less than 10^{-7} s. Slower reactions (to be discussed later) cause dissociation to take place along the ion flight path (not just at the interaction region), which results in asymmetric daughter ion TOF distributions. Because the reaction is fast, the measured abundances are independent of the exact dissociation rate and are only a function of the photon energy and the initial internal energy distribution of the SiCl$_4^+$. We have previously shown that the ion internal energy distribution is generally well-approximated by assuming a faithful transposition of the neutral thermal energy distribution up to the ionic manifold.[10] As a result, the observed breakdown diagram can be modeled by integrating the portion of the thermal energy distribution which, at a given photon energy, lies above the threshold to dissociation. The best-fit curve is determined by varying a single parameter (E_0) and appears in Figure 1. The uncertainty in E_0 is determined by varying the onset above and below the best fit until the modeled curve is clearly no longer an acceptable fit to the data (Figure 1). Thermochemistry derived from this measurement is discussed below.

SiCl$_3$H. The lowest energy dissociation channel of SiCl$_3$H$^+$ is H loss, which, like the Cl loss from SiCl$_4$, produces the SiCl$_3^+$
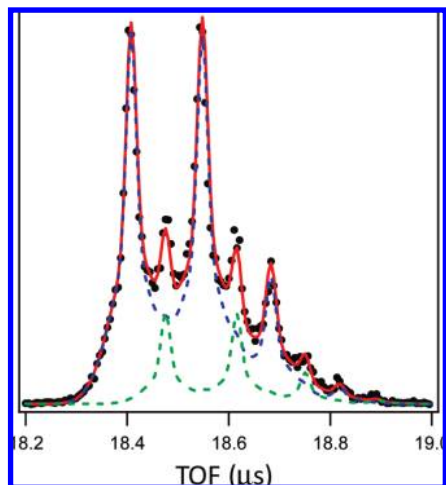
Figure 2. Experimental TOF spectrum (black circles) of $SiCl_3H$ at 11.759 eV photon energy. Ion abundances are derived from the best fit linear combination (red solid line) of the $SiCl_3H^+$ (green dashed line) and $SiCl_3^+$ (blue dashed line) peak shapes. The multiple peaks correspond to Cl and Si isotopes, the contributions of which are fixed at the naturally occurring abundances.

Figure 3. Breakdown diagram of $SiCl_3H^+$ at nominal temperatures of 235 (blue) and 295 K (red). Open and closed circles are experimental abundances. Solid line is the data modeled at the best-fit E_0 and effective temperatures as described in the text. Dashed lines are the modeled data at the edges of the uncertainty limits.

Figure 4. Breakdown diagram of $SiCl_3CH_3^+$. Open and closed circles are experimental abundances. Solid lines are the data modeled at the best-fit E_0 as described in the text. Dashed lines are the modeled data at the edges of the uncertainty limits.

ion. The dissociation is also fast on the time scale of our experiment, and E_0 is roughly determined by the photon energy at which the parent ion disappears. The analysis is slightly complicated by the 1 amu difference between the parent and daughter ions. Peak widths in the TOF spectra are functions of the translational energy distribution of the ions. Parent ion peaks appear as the sum of two Gaussians: a narrow peak due to molecules exiting the inlet needle with kinetic energy preferentially perpendicular to the extraction axis and a broader peak due to molecules that have collided with the walls of the spectrometer and rebounded into the interaction region. In most cases, daughter ion peaks are well-represented by a single Gaussian because the peak width is dominated by the kinetic energy release of the dissociation; however, in the case of a H loss, the hydrogen atom carries away nearly all the kinetic energy in the dissociation, and the daughter ion peak retains the two-component shape of the parent ion peak. In this case, the narrow components of the $SiCl_3H^+$ and $SiCl_3^+$ peaks are resolved, but the broad components are not. Ion abundances are determined by fitting a linear combination of the parent and daughter ion peak shapes to each experimental TOF spectrum (Figure 2), and E_0 is determined from the resulting breakdown diagram (Figure 3) as described above. The parent ion abundance never exceeds about 50% because the ion is only weakly bound, and when the photon energy is equal to the adiabatic ionization energy of the neutral, a large portion of the thermal energy distribution already lies above the barrier to dissociation.

The $SiCl_3H$ data were collected at both room temperature and 235 K; however, the data are best modeled by assuming elevated sample temperatures of 460 and 350 K. For most molecules, such as $SiCl_4$ above, the initial ion internal energy distribution is well-described by a transposition of the neutral thermal energy distribution. However, if the neutral and ion geometries are very different, vertical ionization may result in ion geometries far from the equilibrium structure. These ions will be preferentially created in vibrationally excited states. This appears to be the case here because the $SiCl_3H^+$ geometry has an elongated Si—H bond relative to the neutral, whereas the $SiCl_3$ subgroup is approaching a trigonal planar conformation. These changes in geometry are reflected in significant decreases in the frequencies of numerous normal modes of the ion relative
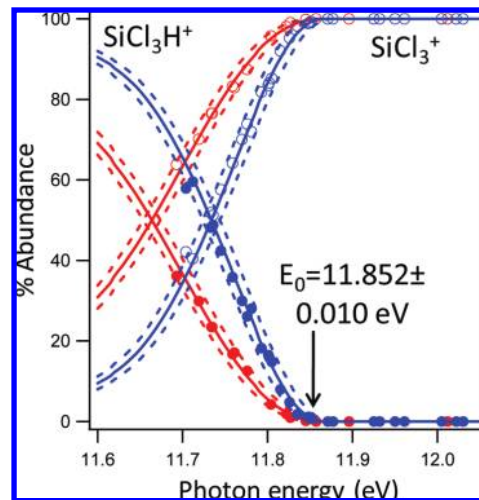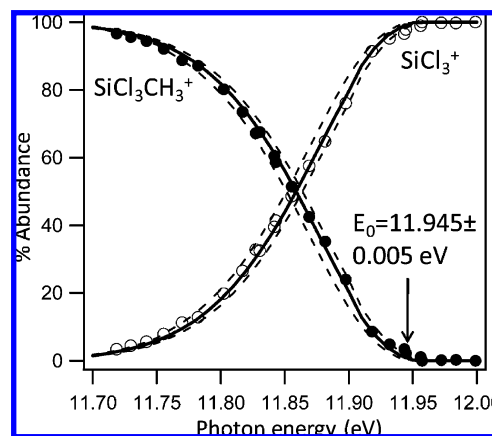
to the same modes in the neutral. Optimized geometries and harmonic frequencies at the B3LYP/6-311++G(d,p) are given in online Supporting Information. We are unable to quantitatively relate the geometry change to the ion internal energy distribution or even reliably predict from given ion and neutral geometries whether the ion energy distribution will differ significantly from that of the neutral. This relationship is potentially an avenue of interest, but it is beyond the scope of this paper.

$SiCl_3CH_3$. The lowest energy dissociation pathway of $SiCl_3CH_3^+$ is methyl loss, analogous to Cl loss from $SiCl_4^+$, which also produces $SiCl_3^+$. To reduce the thermal internal energy distribution, these data were collected with the sample inlet held at 230 K; the breakdown diagram appears in Figure 4. Analysis of the data is identical to that described above for $SiCl_4$. The best fit onset appears in Figure 4, and the thermochemistry derived from this value is discussed below.

A room temperature breakdown diagram was also obtained using the iPEPICO endstation[17] on the VUV beamline at the Swiss Light Source synchrotron facility to take advantage of the extended photon energy range. An electron-impact study[3] on the compound reported two dissociation pathways: methyl
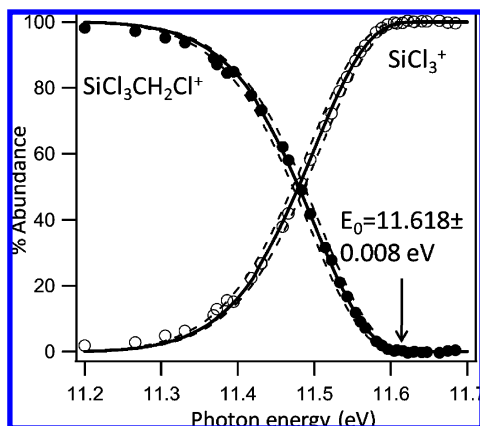
Thermochemistry of SiCl$_3$R, SiCl$_3^+$, and SiCl$_3^\bullet$

J. Phys. Chem. A, Vol. 113, No. 34, 2009 **9461**

Figure 5. Breakdown diagram of SiCl$_3$CH$_2$Cl$^+$. Open and closed circles are experimental abundances. Solid lines are the data modeled at the best-fit E_0 as described in the text. Dashed lines are the modeled data at the edges of the uncertainty limits.
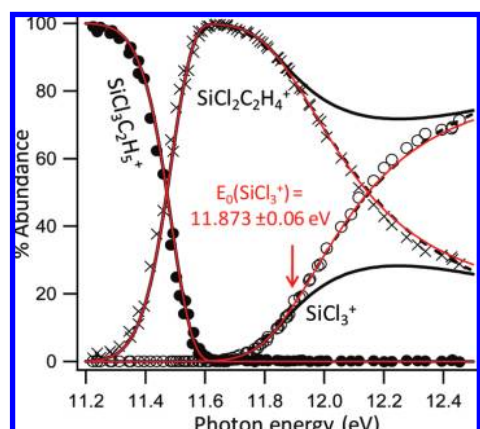

Figure 6. Breakdown diagram of SiCl$_3$C$_2$H$_5^+$. Points are experimental ion abundances for SiCl$_3$C$_2$H$_5^+$ (●), SiCl$_2$C$_2$H$_4^+$ (×), and SiCl$_3^+$ (○). Curves are best-fit simulations using RRKM (− −) or SSACM with two (solid black line) or three (red line) adjustable parameters. The indicated E_0 is obtained from the three-parameter SSACM fit.

loss at 11.9 eV and appearance of CH$_3^+$ (along with SiCl$_3^\bullet$ coproduct) at 15.0 eV. Because the difference between the onsets must be equal to the difference in the ionization energies of the two radical species, measurement of the second onset would allow for determination of the SiCl$_3^\bullet$ radical heat of formation. Unfortunately, only a minor methyl ion channel was observed as a result of photoionization, at significantly higher energy and in competition with numerous other channels, preventing accurate determination of the onset.

SiCl$_3$CH$_2$Cl. Unlike SiCl$_4$ and SiCl$_3$CH$_3$, SiCl$_3$CH$_2$Cl has not been the subject of any prior electron impact or photoionization studies. We observe that, similar to those two compounds, the lowest energy dissociation channel is a simple Si−C bond cleavage to produce SiCl$_3^+$ and CH$_2$Cl$^\bullet$. The breakdown diagram (collected at 250 K) appears in Figure 5. Analysis of the data is identical to that described above. The best fit onset appears in Figure 5, and the thermochemistry derived from this value is discussed below.

SiCl$_3$C$_2$H$_5$. Previous electron impact studies on SiCl$_3$C$_2$H$_5$ report the lowest energy dissociation channel to be Si−C bond cleavage. However, as shown in the breakdown diagram in Figure 6, photoionization results in SiCl$_2$C$_2$H$_4^+$, the product of HCl loss, as the lowest energy channel. At a few hundred millielectronvolts higher photon energy, the SiCl$_3^+$ daughter appears and, because the loose transition state of the simple
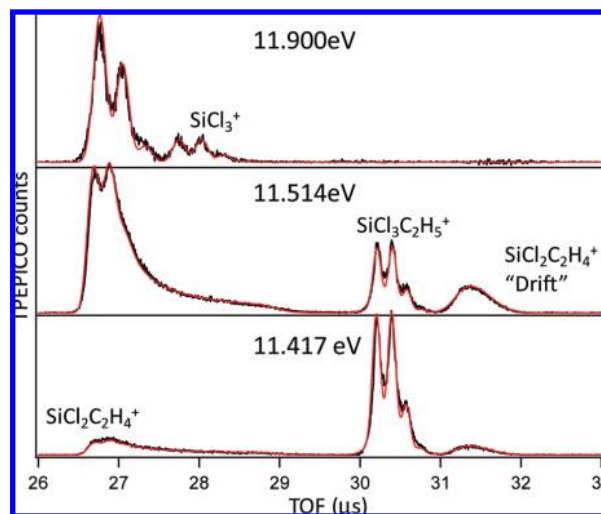

Figure 7. Representative experimental (black line) and simulated (red line) TOF spectra of the dissociation of SiCl$_3$C$_2$H$_5^+$ at the indicated photon energies.

bond cleavage is entropically favored over the tight transition state associated with HCl loss, quickly grows in to dominate the product branching. The analysis to determine the E_0 of the SiCl$_3^+$ channel is different from those discussed above for two reasons: First, to determine the higher energy onset, the relative rates of the parallel channels must be properly modeled. Second, the HCl loss channel occurs slowly on the time scale of our experiment, as indicated by the highly asymmetric daughter ion peak apparent in Figure 7, and the metastability of SiCl$_3$C$_2$H$_5^+$ must be considered when modeling the data.

In this case, the solution to one of these problems informs the other. The dissociation rate of SiCl$_3$C$_2$H$_5^+$ is reflected in the shape of the asymmetric daughter peak as well as in the abundance of the "drift" peak (the result of ions dissociating in the field-free drift region before the final deceleration region). By finding a best-fit model of the TOF spectra using statistical theory, the rate of HCl loss is directly measured over several orders of magnitude (roughly between 10^3 and 10^7 s^{-1}) and can be reliably extrapolated to higher energies. The measured relative abundance of SiCl$_3^+$ to SiCl$_2$C$_2$H$_4^+$ indicates the relative rates of the two channels and defines the rate of the SiCl$_3^+$ channel at ion internal energies where SiCl$_3^+$ product is detected (because our detection limit is ∼1% abundance, this is roughly at and above the internal energy where the SiCl$_3^+$ rate reaches 1% of the HCl loss rate). Unfortunately, determining the higher energy onset still requires extrapolation of the SiCl$_3^+$ rate curve down to threshold.

As is typical for a bimolecular elimination, the HCl loss channel passes through an energetic barrier along the reaction coordinate. Because of the barrier, the HCl loss product ion will not necessarily be observed at its thermochemical threshold to dissociation so that the derived E_0 is only an upper limit for the thermochemical threshold. Because this channel passes over an energetic maximum and therefore has a well-defined transition state geometry, the rate should be well-described using RRKM theory.[18] Excellent fits to the TOF spectra (Figure 7) are found by modeling the dissociation using RRKM theory with the transition state defined by the calculated harmonic vibrational frequencies and optimizing the barrier to dissociation. The good fits, in which only the assumed E_0 is varied, indicate that the portion of the rate curve measurable by our experiment is correctly reproduced in the modeling. Similar fits are found whether or not the modeling includes a tunneling rate as

described using an Eckart barrier.[18] Importantly, the extrapolated high energy portion of the rate curve (the region that is important to determining the higher energy onset) is largely independent of whether tunneling is included in the modeling.

The second onset is a simple bond cleavage and proceeds with no reverse barrier. As such, it does not have a well-defined transition state. Nonetheless, we have previously modeled the rate of this type of dissociation using RRKM theory by treating the vibrational frequencies of the transitional modes (reactant vibrations which become orbital motions of the products) as optimizable parameters in calculating the number of states of the transition state. In this case, RRKM provides a perfect fit to the experimental data (Figure 6), suggesting an E_0 of 11.764 $\pm$ 0.04 eV. However, due to the competitive shift of the higher energy channel, the experiment provides information about of the higher energy channel only at rates exceeding about $k(E)$ = 4 × 10^5 s^{-1}. Although the lower energy portion of the rate curve, which is critical to accurately determining E_0, can be extrapolated using RRKM theory, RRKM theory has been shown to incorrectly model reaction rates of barrierless ionic dissociations near threshold, even while it correctly models the higher energy rates.[19,20]

More appropriate versions of statistical theory, variational transition state theory,[21,22] or the statistical adiabatic channel model (SACM),[23,24] are arduous to apply to a system with this complexity, to the point of being intractable. Instead, we use a simplified version of SACM (SSACM)[20] previously shown to correctly extrapolate the rates of barrierless ionic dissociations down to threshold.[19,20] The best-fit simulation of the data using SSACM appears in Figure 6 and suggests an E_0 that is 90 meV higher than does RRKM. SSACM provides an excellent fit at low energies but deviates significantly from the experimental data at higher energies. The explanation for this deviation and a solution to it requires a description of SSACM; a brief summary of the model follows and a more detailed explanation can be found elsewhere.[19,20,25]

SSACM posits that the rate of a barrierless ionic dissociation will deviate from the rate predicted by orbiting transition state phase space theory (PST)[26] only due to anisotropy of the potential surface along the reaction coordinate. The restriction of product orbital motion due to increased anisotropy is approximated by introducing a "rigidity factor" (f_{rigid}) into the calculation of the PST number of states such that

$$N_{SSACM} = (\rho_{conserved})*(N_{PST} f_{rigid})$$

where N_{SSACM} is the SSACM number of states, N_{PST} is the PST number of states of the orbital motion of the products, $\rho_{conserved}$ is the density of states of the conserved modes, and the asterisk (*) indicates a convolution. The functional form of f_{rigid} is not derived but, rather, is chosen to fit accurately calculated or measured $k(E)$ functions over a large energy range and to extrapolate to the PST limit as $E \rightarrow 0$. We have previously employed a simple exponential[19]

$$f_{rigid}(E) = e^{(-(E-E_0)/c1)}$$

where E is the internal energy of the dissociating ion and c1 is an optimizable parameter nominally dependent on the isotropic polarizability of the neutral product fragment. This form of $f_{rigid}(E)$, which is essentially a first-order correction to PST, approaches zero as the ion internal energy increases, and above some energy, f_{rigid} becomes so small that the transitional modes
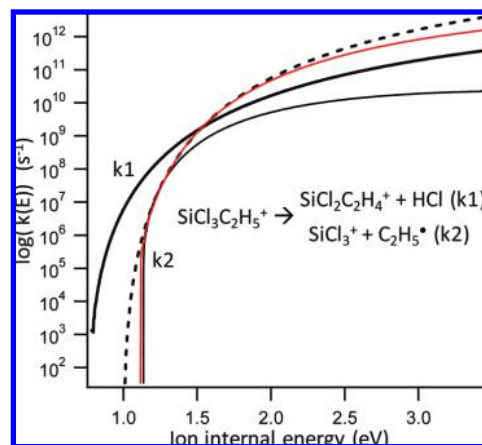

Figure 8. Energy-specific rate curves for the dissociation of SiCl$_3$C$_2$H$_5$$^+$ for HCl loss (thick, black line labeled as k1) and for Si—C bond cleavage modeled either by RRKM (dashed line), two-parameter SSACM (thin black line), or three-parameter SSACM (red line).

make zero contribution to the number of states. This is clearly not physical and explains why the SSACM rate curve underestimates the true rate curve at higher ion internal energies; it is ignoring any contribution from 5 out of 27 modes.

This effect can be mitigated by placing a nonzero lower limit on f_{rigid}, such as[20]

$$f_{rigid}(E) = e^{(-(E-E_0)/c1)} + c2(1 - e^{-(E-E_0)/c1})$$

where both c1 and c2 are treated as optimizable parameters. In this case, introducing a third parameter (in addition to c1 and E_0) does not significantly increase the flexibility of the model, and E_0 can still be well and uniquely defined. A good fit to the data (even at only low ion internal energies) can be found only for values of c2 < 0.002, and E_0 varies by only 25 meV throughout this range. The best fit, found when c1 = 5.6 meV, c2 = 0.001, and E_0 = 11.873 $\pm$ 0.06 eV, is shown in Figure 6. The dissociation rate curve defined by this three-parameter model is shown in Figure 8; note that at low energies, it agrees with the two-parameter SSACM model, and at higher energies, it agrees with the RRKM model. In general, we would not find a model with so many adjustable parameters reliable.[27] Here, we are effectively relying on two-parameter SSACM to define the rate curve at lower energies (and therefore, E_0), RRKM to define the curve at higher energies, and the three-parameter fit as a switching function between them.

We emphasize that although RRKM provides an excellent description of the experimental data, derivation of E_0 here requires an extrapolation to dissociation rates unobservable by the experiment, and RRKM has been shown to be unreliable for this extrapolation.[19] The excellent RRKM fit to the data is then deceptive as to the accuracy of the derived E_0. We rely on SSACM here, despite its clear deficiencies at higher internal energies because it has been shown to correctly extrapolate barrierless ionic dissociation rate curves down to threshold. The RRKM results are presented to show the extent to which the derived competitive shift depends on the rate theory employed.

SiCl$_3$C$_2$H$_3$. The dissociation of internally excited SiCl$_3$C$_2$H$_3$$^+$ is very similar to that of SiCl$_3$C$_2$H$_5$$^+$. The lowest energy channel is HCl loss, and at higher energies, the Si—C bond cleaves to produce SiCl$_3$$^+$. The analysis is similar to that described above for SiCl$_3$C$_2$H$_5$$^+$. RRKM theory fits the data well and suggests a competitive shift of the higher energy channel 150 meV larger

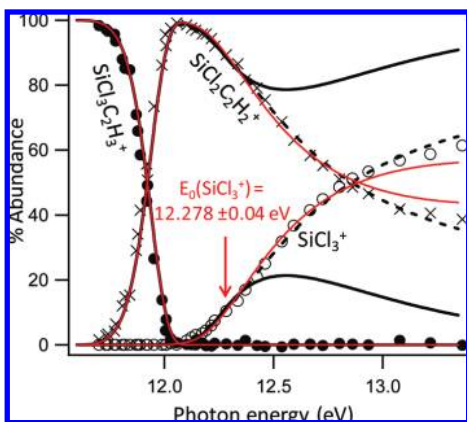**Figure 9.** Breakdown diagram of $SiCl_3C_2H_3^+$. Points are experimental ion abundances for $SiCl_3C_2H_3^+$ (●), $SiCl_2C_2H_2^+$ (×), and $SiCl_3^+$ (○). Curves are best-fit simulations using RRKM (− −) or SSACM with two (solid black line) or three (red line) adjustable parameters. The indicated E_0 is for the vinyl loss channel reaction modeled by the three-parameter SSACM fit.
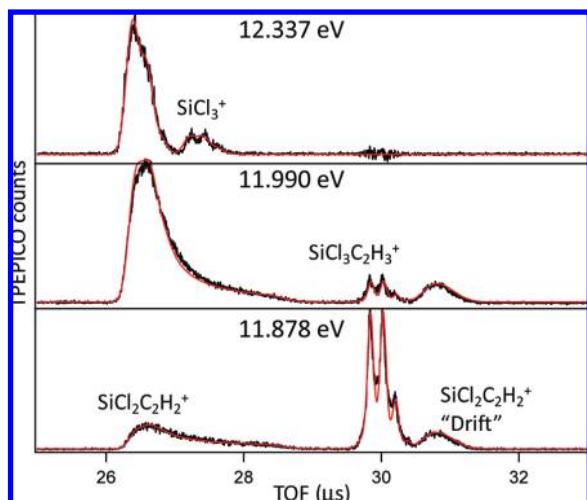

Figure 10. Representative experimental (black line) and simulated (red line) TOF spectra of the dissociation of $SiCl_3C_2H_3^+$ at the indicated photon energies.

Figure 11. Energy-specific rate curves for the dissociation of $SiCl_3C_2H_3^+$ for HCl loss (thick, black line, k1) and for Si−C bond cleavage modeled either by RRKM (− −), two-parameter SSACM (thin black line), or three-parameter SSACM (red line).

Figure 12. Breakdown diagram of $Si_2Cl_6^+$. Points are experimental ion abundances for $Si_2Cl_6^+$ (●), $SiCl_2^+$ (×), and $SiCl_3^+$ (○). Curves are best-fit simulations using RRKM (− −) or SSACM with two (solid black line) or three (red line) adjustable parameters.

than does SSACM. Two-parameter SSACM provides a good fit to the data only at lower ion internal energies, whereas a three-parameter SSACM model fits the full range of the data. The best fit (Figures 9 and 10) is found when c1 = 10 meV, c2 = 0.006, and E_0 = 12.278 ± 0.05 eV. The rate curves of the competing dissociations are shown in Figure 11.

It is not immediately clear in HCl loss from either $SiCl_3C_2H_3^+$ or $SiCl_3C_2H_5^+$ whether the channel is a product of 1, 2 or 1, 3 elimination. In both cases, the product of 1, 2 elimination is the more stable at the G3 level of calculation, and both elimination pathways are endothermic. Additionally, we are unable to locate a transition state to 1, 3 elimination on the potential surface and assume that the channel proceeds by 1, 2 elimination. The geometry of the four-center transition state for the 1, 2 elimination is very similar to that calculated for HX loss in a number of other systems.[28−30] It is unclear why, if the 1, 2 elimination occurs, no HCl loss is seen in either $SiCl_3CH_3$ or $SiCl_3CH_2Cl$. The immediate assumption would be that the formation of a primary radical causes these channels to be energetically unfavorable; however, calculations at the G3 level suggest that both the final product state and the transition state
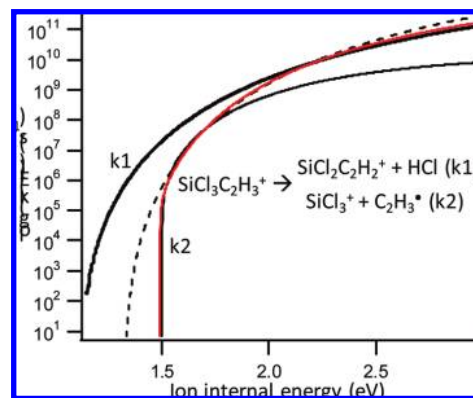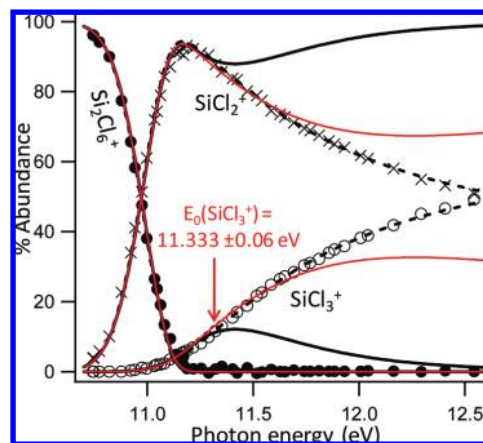
to 1, 2 elimination are *lower* in energy relative to the dissociating ion in both $SiCl_3CH_3^+$ and $SiCl_3CH_2Cl^+$ than in $SiCl_3C_2H_3^+$ or $SiCl_3C_2H_5^+$.

Si_2Cl_6. Two previous electron impact studies[3,4] of Si_2Cl_6 report Si−Si bond cleavage as the lowest energy channel. As shown in the breakdown diagram (Figure 12), the lowest energy channel as a result of photoionization is a rearrangement to form $SiCl_2^+$ and $SiCl_4$. Only at somewhat higher energies does the Si−Si bond break to yield $SiCl_3^+$ and $SiCl_3^\bullet$. Although mechanistically distinct from the HCl loss in $SiCl_3C_2H_5$ and $SiCl_3C_2H_3$, the analysis of the data is nearly identical. The rate of the slow rearrangement is determined from the shape of the asymmetric daughter peak in the TOF spectra (Figure 13) using RRKM theory. E_0 of the higher energy channel is determined by modeling the rate of the simple bond cleavage using either two- or three-parameter SSACM (both yield the same onset to well within uncertainty). Modeling the higher energy channel rate using RRKM theory provides a perfect fit to the data; however, again it suggests a larger competitive shift than does SSACM.

The best-fit rate curves of the $Si_2Cl_6^+$ dissociation appear in Figure 14. As in the $SiCl_3C_2H_5^+$ and $SiCl_3C_2H_3^+$ dissociations, RRKM theory correctly models the rate curve at higher ion internal energies, whereas two-parameter SSACM models the rate curve at lower ion internal energies and three-parameter SSACM over a wider range of energies, although still imperfectly at higher energies. The best three-parameter fit is found
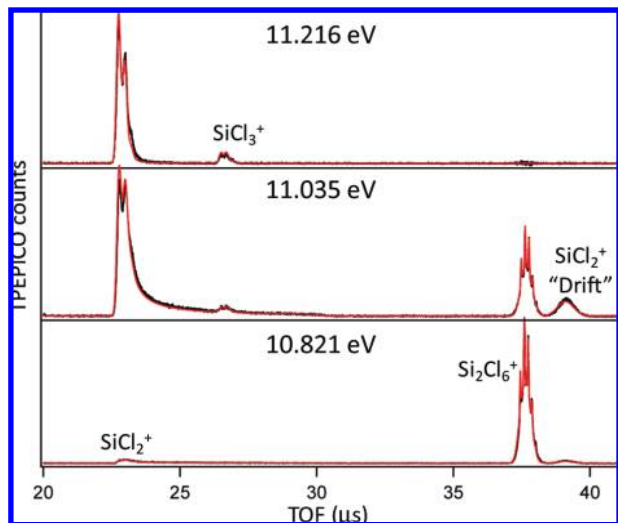
9464 *J. Phys. Chem. A, Vol. 113, No. 34, 2009*

Shuman et al.

Figure 13. Representative experimental (black line) and simulated (red line) TOF spectra of the dissociation of $Si_2Cl_6^+$ at the indicated photon energies.
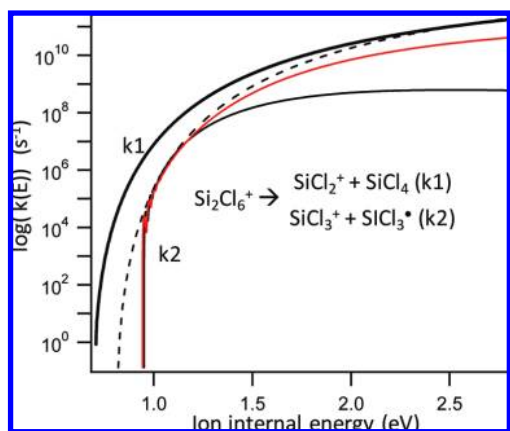

Figure 14. Energy-specific rate curves for the dissociation of $Si_2Cl_6^+$ for rearrangement to form $SiCl_2^+$ (thick black line) and for Si−Si bond cleavage modeled by RRKM (− −), two-parameter SSACM (thin black line), or three-parameter SSACM (red line).

TABLE 1: Ancillary Heats of Formation (kJ mol^{-1})

species	ΔH_f^0 0 K^a	$H_{298K} - H_{0K}$	ΔH_f^0 298 K
SiCl$_4$	−660.1	18.9	−662.8 ± 2.0^b
CH$_3^\bullet$	149.9^c	10.5^c	146.7 ± 0.3^d
CH$_2$Cl$^\bullet$	123.7	11.7	121.3 ± 4.2^e
C$_2$H$_5^\bullet$	132.3^c	11.7^c	120.7 ± 1.0^c
C$_2$H$_3^\bullet$	298.9^f	10.6	295.4 ± 1.7^f

^{a} Uncertainties in the 0 K values are the same as the 298 K values unless otherwise noted. ^{b} The average value taken from Wang and He, Chase, and Walsh.[1,5,6] ^{c} From Bodi et al.[34] ^{d} From Ruscic et al.[35] ^{e} From Lazarou et al. and DeMore et al.[36,37] ^{f} From Parthiban and Martin, and Kaiser and Wallington.[38,39]

when $E_0 = 11.333 \pm 0.06$ eV, c1 = 3.5 meV, and c2 = 0.0002. Thermochemistry derived from the measured onset is discussed below.

Thermochemistry

Because the heats of formation of SiCl$_4$ and Cl$^\bullet$ are well-known (Table 1), the E_0 for SiCl$_4$ dissociation determines the 0 K heat of formation of SiCl$_3^+$ (Table 2). This value can be converted to the 298 K heat of formation ($\Delta H_{f,298K}^0 = 435.6 \pm 2.0$ kJ mol^{-1}) by the standard thermochemical cycle (by

convention, the e$^-$ is treated as remaining at 0 K). An evaluation of older experimental determinations suggested 427 ± 13 kJ mol^{-1},[31] which is, within the experimental uncertainty, equal to our value, but the latter is far more precise. An older calculation at the CCSD(T)/AVQZ level reports 421 kJ mol^{-1},[32] significantly off the current result, but a recent G3(CC) calculation (439.3 kJ mol^{-1}) is in excellent agreement.[1]

Using SiCl$_3^+$ as an anchor, the E_0's measured for SiCl$_3$H, SiCl$_3$CH$_3$, SiCl$_3$CH$_2$Cl, SiCl$_3$C$_2$H$_5$, and SiCl$_3$C$_2$H$_3$ each yield the heat of formation of the neutral species (Table 2). Of these compounds, prior experimental heats of formation exist only for SiCl$_3$H and SiCl$_3$CH$_3$. The NIST−JANAF compilation[5] reports the SiCl$_3$H 298 K heat of formation as -496.2 ± 4.2 kJ mol^{-1}, and Walsh[6] suggests an evaluated number of -499 ± 7 kJ mol^{-1}, both in excellent agreement with our experimental value of -494.4 ± 2.3 kJ mol^{-1}. On the other hand, NIST−JANAF reports the SiCl$_3$CH$_3$ $\Delta H_{f,298K}^0$ as -529 kJ mol^{-1}, nearly 50 kJ mol^{-1} more positive than the value reported here.[5] These are the first reliable heats of formation for most of these species and provide a means to evaluate calculated results. We have calculated the heats of formation of each of these species by employing isodesmic reactions and two common model chemistries, G3 and CBS-QB3 (Table 3). The values derived using the two model chemistries are in excellent agreement with one another (differing by less than 3 kJ mol^{-1} in all cases), and their averaged value is in excellent agreement with the experimental values (differing by just −3.1 (SiCl$_3$CH$_2$Cl), −2.1 (SiCl$_3$CH$_3$), 2.6 (SiCl$_3$C$_2$H$_5$), 3.4 (SiCl$_3$C$_2$H$_3$), and 5.8 (SiCl$_3$H) kJ mol^{-1}). We note that if the E_0's derived using RRKM theory for the SiCl$_3$C$_2$H$_5$ and SiCl$_2$C$_2$H$_3$ systems were accurate, the calculated heats of formation would be 9 and 11 kJ mol^{-1} too positive, respectively. This supports our initial assumption that, although RRKM theory is able to correctly model the dissociation rate throughout the experimental region, the extrapolation to lower ion internal energies overestimates the competitive shift.

The Si$_2$Cl$_6$ system poses a problem because neither the heat of formation of Si$_2$Cl$_6$ nor SiCl$_3^\bullet$ is well-known. Instead, we rely on a calculated value of the Si$_2$Cl$_6$ heat of formation using the same scheme of isodesmic reactions that accurately reproduces the experimental heats of formation of the other SiCl$_3$R derivatives (Table 3). Using the average of two isodesmic reactions, each calculated by G3 and CBS-QB3, we suggest that Si$_2$Cl$_6$ $\Delta H_{f,0K}^0 = -979 \pm 6$ kJ mol^{-1}, $\Delta H_{f,298K}^0 = -980 \pm 6$ kJ mol^{-1}. Assigning uncertainties to calculated values is a somewhat subjective task. The reported uncertainty assumes an uncertainty of 10 kJ mol^{-1} in each G3 and CBS-QB3 calculated isodesmic heat of reaction and treats both the two model chemistries and the two isodesmic reactions as independent of each other, yielding four determinations of the heat of formation of Si$_2$Cl$_6$. The number appears reasonable in consideration of the high accuracy with which the same scheme reproduces the experimental heats of formation of similar compounds. With the Si$_2$Cl$_6$ heat of formation defined, the measured E_0 determines the heat of formation of the SiCl$_3$ radical to be $\Delta H_{f,0K}^0 = -322 \pm 8$ kJ mol^{-1}, $\Delta H_{f,298K}^0 = -323 \pm 8$ kJ mol^{-1}. This value is significantly different from the NIST−JANAF result (-390 ± 17)[5] and also in somewhat poor agreement with the value suggested by Walsh (-335 ± 8 kJ mol^{-1}).[6] However, the Walsh value is based on accepting SiCl$_3$H $\Delta H_{f,298K}^0 = -499.1 \pm 7$ kJ mol^{-1}. Adopting the more accurate heat of formation determined here adjusts the Walsh SiCl$_3^\bullet$ heat of formation to -330 ± 8 kJ mol^{-1}, mitigating the discrepancy. Theoretical determinations of the SiCl$_3^\bullet$ heat of formation range between −315 and 320 kJ

TABLE 2: Heats of Formation Derived from $SiCl_3R \rightarrow SiCl_3^+ + R^{\bullet}$ E_0's

species	reaction products	measured onset (eV)	ΔH_f^0 0 K (kJ mol⁻¹)	$H_{298K} - H_{0K}$	ΔH_f^0 298 K (kJ mol⁻¹)	ΔH_f^0 298 K (lit.)
$SiCl_3^+$	$SiCl_3^+ + Cl^{\bullet}$	12.615 ± 0.005	437.1 ± 2.0	15.6	435.6 ± 2.0	439.3[a], 427 ± 13[b], 421[c]
$SiCl_3H$	$SiCl_3^+ + H^{\bullet}$	11.852 ± 0.010	−489.6 ± 2.3	16.3	−494.4 ± 2.3	−488.5[a], −496.2 ± 4.2[d], −499.2 ± 7[e]
$SiCl_3CH_3$	$SiCl_3^+ + CH_3^{\bullet}$	11.945 ± 0.005	−566.5 ± 2.2	21.3	−575.8 ± 2.2	−529[d]
$SiCl_3CH_2Cl$	$SiCl_3^+ + CH_2Cl^{\bullet}$	11.618 ± 0.008	−560.3 ± 5.6	23.9	−567.4 ± 5.6	
$SiCl_3C_2H_5$	$SiCl_3^+ + C_2H_5^{\bullet}$	11.873 ± 0.06	−576.2 ± 6.1	25.0	−591.5 ± 6.1	
$SiCl_3C_2H_3$	$SiCl_3^+ + C_2H_3^{\bullet}$	12.278 ± 0.05	−448.7 ± 5.4	24.2	−456.3 ± 5.4	
$SiCl_3^{\bullet}$	$SiCl_3^+ + SiCl_3^{\bullet}$	11.333 ± 0.06	−320 ± 8	16.2	−321 ± 8	−330 ± 8,[e] −390 ± 17,[d] −326 ± 12[b], −317.3[a]

[a] Calculation by Wang and He.[1] [b] Evaluation by Weber and Armentrout.[31] [c] From Basuchlicher and Partridge.[32] [d] From NIST−JANAF.[5] [e] From Walsh.[6]

TABLE 3: Heats of Formation of SiCl₃R by Isodesmic Reaction Calculations[a] (kJ mol⁻¹)

species	reaction	ΔH_r G3	ΔH_r CBS-QB3	$\Delta H_{f,0k}^0$[b]	deviation from exp[c]
$SiCl_3CH_3$	$4SiCl_3CH_3 \rightarrow Si(CH_3)_4 + 3SiCl_4$	86.0	88.1	−567.9	−1.7
$SiCl_3H$	$SiCl_3H + SiH_3Cl \rightarrow SiCl_4 + SiH_4$	−8.9	−6.5	−483.2	6.8
	$SiCl_3H + (2/3)SiH_3CH_3 \rightarrow SiH_3Cl + (2/3)SiCl_3CH_3$	−10.7	−10.6	−486.7	3.3
$SiCl_3CH_2Cl$	$SiCl_3CH_2Cl + (3/4)SiH_4 \rightarrow (3/4)SiCl_4 + SiH_3CH_2Cl$	21.7	20.3	−565.5	−4.6
	$SiCl_3CH_2Cl + SiClH_3 \rightarrow SiCl_4 + SiH_3CH_2Cl$	12.8	13.8	−561.1	−0.2
$SiCl_3C_2H_5$	$SiCl_3C_2H_5 + CH_4 \rightarrow SiCl_3CH_3 + C_2H_6$	6.9	6.4	−574.5	2.4
$SiCl_3C_2H_3$	$SiCl_3C_2H_3 + CH_4 \rightarrow SiCl_3CH_3 + C_2H_4$	7.4	7.2	−446.1	3.4
Si_2Cl_6	$Si_2Cl_6 + (3/2)SiH_4 \rightarrow Si_2H_6 + (3/2)SiCl_4$	18.9	21.0	−984.1	
	$Si_2Cl_6 + (3/2)Si(CH_3)_4 \rightarrow Si_2(CH_3)_6 + (3/2)SiCl_4$	25.0	28.2	−974.2	

[a] Detailed results of calculations and ancillary heats of formation available as online Supporting Information. [b] Determined using the averaged ΔH_r of the two model chemistries. [c] Calculated $\Delta H_{f,0k}^0$ compared to experimental values from Table 2.

TABLE 4: Si−R Bond Dissociation Energies of SiCl₃R

SiCl₃−R	BDE 0 K (kJ mol⁻¹)	BDE 298 K[a] (kJ mol⁻¹)	lit. BDE 298 K
$SiCl_3-Cl$	458 ± 8	461	462 ± 9,[b] 465.7 ± 4.2[c]
$SiCl_3-H$	384 ± 9	391	382 ± 5,[d] 395 ± 5[b]
$SiCl_3-CH_3$	394 ± 8	399	
$SiCl_3-CH_2Cl$	362 ± 8	366	
$SiCl_3-C_2H_5$	387 ± 10	391	
$SiCl_3-C_2H_3$	426 ± 9	428	
$SiCl_3-SiCl_3$	334 ± 9	334	

[a] Uncertainties in the 298 K values are the same as the 0 K values unless otherwise noted. [b] From Walsh.[40] [c] From Hildenbrand et al.[41] [d] From Walsh.[42]

TABLE 5: Heats of Formation (kJ mol⁻¹) of SiH₃R by Isodesmic Reaction Calculations $SiH_3R + SiCl_4 \rightarrow SiCl_3R + SiCl_3H$

species	ΔH_r G3	ΔH_r CBS-QB3	$\Delta H_{f,0k}^0$	$H_{298K} - H_{0K}$	$\Delta H_{f,298k}^0$	lit. $\Delta H_{f,298k}^0$
SiH_4	8.9	6.5	19.2	10.5	30.7	37.7[a]
SiH_3CH_3	−18.9	−20.2	−19.2	13.5	−35.4	−28.9[b]
SiH_3CH_2Cl	−12.8	−13.8	−20.1	14.8	−35.3	−35.6[b]
$SiH_3C_2H_5$	−24.7	−25.9	−24.1	16.6	−46.6	
$SiH_3C_2H_3$	−17.0	−17.7	95.5	15.2	79.9	
SiH_3SiCl_3	−0.9	−1.9	540.7	24.1	531.9	

[a] Calculated by Karton and Martin.[33] [b] Calculated by Grant and Dixon.[2]

mol⁻¹,[1] in reasonable agreement with the value reported here. Adopting this heat of formation sets the adiabatic IE of SiCl₃˙ at 7.87 ± 0.08 eV. The bond dissociation enthalpy (BDE) of each of the neutral species investigated here is equal to the difference of the respective E_0 and the IE of SiCl₃˙; the derived BDE values appear in Table 4.

The experimentally determined heats of formation of the trichlorosilane species may be used in isodesmic reaction calculations to accurately determine the heats of formation of saturated alkyl silanes of interest in chemical hydrogen storage systems.[2] The isodesmic reactions and resulting heats of formation appear in Table 5. The heats of formation of three of the compounds—SiH₄, SiH₃CH₃, and SiH₃CH₂Cl—may be compared to the values of Dixon et al.[2] and Martin et al.[33] calculated using higher level ab initio methods, and are in reasonable agreement.

Summary

The 0 K onsets of $SiCl_3R \rightarrow SiCl_3^+ + R^{\bullet}$ (R = Cl, H, CH₃, CH₂Cl, C₂H₅, C₂H₃, SiCl₃) have been measured by TPEPICO spectroscopy. From these onsets, the heats of formation of

SiCl₃⁺, SiCl₃H, SiCl₃CH₃, SiCl₃CH₂Cl, SiCl₂C₂H₅, and SiCl₃C₂H₃ were derived. A series of isodesmic reactions calculated using the G3 and CBS-QB3 model chemistries were shown to accurately reproduce the experimental thermochemistry, and this scheme was used to determine to heat of formation of Si₂Cl₆. Using the calculated Si₂Cl₆ heat of formation and experimentally determined onset, the heat of formation of SiCl₃˙ was determined. From this value, the adiabatic ionization energy of SiCl₃˙ along with the Si−R bond dissociation enthalpies of the six neutral molecules investigated were derived. Finally, the heats of formation of the analogous series of SiH₃R were calculated using isodesmic reactions.

Supporting Information Available: Calculated energies and experimental heats of formation used in the isodesmic reactions as well as calculated neutral and ion harmonic frequencies used in the rate analysis are made available as Supporting Informa-

tion. This information is available free of charge via the Internet at http://pubs.acs.org.

References and Notes

(1) Wang, L. M.; He, Y. L. *Int. J. Mass Spectrom.* **2008**, *276* (1), 56–76.

(2) Grant, D. J.; Dixon, D. A. *J. Phys. Chem. A* **2009**, *113* (15), 3656–3661.

(3) Steele, W. C.; Stone, F. G. A.; Nichols, L. D. *J. Am. Chem. Soc.* **1962**, *84* (23), 4441.

(4) Potzinger, P.; Ritter, A.; Krause, J. *Z. Naturforsch.* **1975**, *30a*, 347–355.

(5) Chase, M. W. *NIST−JANAF Thermochemical Tables*, 4th ed.; American Institute of Physics: New York, 1998.

(6) Walsh, R. *J. Chem. Soc.-Faraday Trans. I* **1983**, *79*, 2233–2248.

(7) Davalos, J. Z.; Baer, T. *J. Phys. Chem. A* **2006**, *110*, 8572–8579.

(8) Baer, T.; Li, Y. *Int. J. Mass Spectrom.* **2002**, *219*, 381–389.

(9) Sztáray, B.; Baer, T. *Rev. Sci. Instrum.* **2003**, *74*, 3763–3768.

(10) Kercher, J. P.; Stevens, W.; Gengeliczki, Z.; Baer, T. *Int. J. Mass Spectrom.* **2007**, *267*, 159–166.

(11) Frisch, M. J.; Trucks, G. W.; Schlegel, H. B.; Scuseria, G. E.; Robb, M. A.; Cheeseman, J. R.; Montgomery, J. A., Jr.; ; T.; Kudin, K. N.; Burant, J. C.; Millam, J. M.; Iyengar, S. S.; Tomasi, J.; Barone, V.; Mennucci, B.; Cossi, M.; Scalmani, G.; Rega, N.; Petersson, G. A.; Nakatsuji, H.; Hada, M.; Ehara, M.; Toyota, K.; Fukuda, R.; Hasegawa, J.; Ishida, M.; Nakajima, T.; Honda, Y.; Kitao, O.; Nakai, H.; Klene, M.; Li, X.; Knox, J. E.; Hratchian, H. P.; Cross, J. B.; Bakken, V.; Adamo, C.; Jaramillo, J.; Gomperts, R.; Stratmann, R. E.; Yazyev, O.; Austin, A. J.; Cammi, R.; Pomelli, C.; Ochterski, J. W.; Ayala, P. Y.; Morokuma, K.; Voth, G. A.; Salvador, P.; Dannenberg, J. J.; Zakrzewski, V. G.; Dapprich, S.; Daniels, A. D.; Strain, M. C.; Farkas, O.; Malick, D. K.; Rabuck, A. D.; Raghavachari, K.; Foresman, J. B.; Ortiz, J. V.; Cui, Q.; Baboul, A. G.; Clifford, S.; Cioslowski, J.; Stefanov, B. B.; Liu, G.; Liashenko, A.; Piskorz, P.; Komaromi, I.; Martin, R. L.; Fox, D. J.; Keith, T.; Al-Laham, M. A.; Peng, C. Y.; Nanayakkara, A.; Challacombe, M.; Gill, P. M. W.; Johnson, B.; Chen, W.; Wong, M. W.; Gonzalez, C.; Pople, J. A. *Gaussian03, Revision C.02*; Gaussian, Inc.: Wallingford, CT, 2004.

(12) Merrick, J. P.; Moran, D.; Radom, L. *J. Phys. Chem. A* **2007**, *111* (11683), 11683–11700.

(13) Curtiss, L. A.; Raghavachari, K.; Redfern, P. C.; Rassolov, V.; Pople, J. A. *J. Chem. Phys.* **1998**, *109* (18), 7764–7776.

(14) Montgomery, J. A.; Frisch, M. J.; Ochterski, J. W.; Petersson, G. A. *J. Chem. Phys.* **2000**, *112* (15), 6532–6542.

(15) Cooper, L.; Rennie, E. E.; Shpinkova, L. G.; Holland, D. M. P.; Shaw, D. A. *Int. J. Mass Spectrom.* **2002**, *220* (3), 359–374.

(16) Steiner, B. W.; Giese, C. F.; Inghram, M. G. *J. Chem. Phys.* **1961**, *34*, 189–220.

(17) Bodi, A.; Johnson, M.; Gerber, T.; Gengeliczki, Z.; Sztáray, B.; Baer, T. *Rev. Sci. Instrum.* **2009**, *80*, 034101-1−034101/7.

(18) Baer, T.; Hase, W. L. *Unimolecular Reaction Dynamics: Theory and Experiments*; Oxford University Press: New York, 1996.

(19) Stevens, W.; Sztáray, B.; Shuman, N.; Baer, T.; Troe, J. *J. Phys. Chem. A* **2009**, *113*, 573–582.

(20) Troe, J.; Ushakov, V. G.; Viggiano, A. A. *J. Phys. Chem. A* **2006**, *110*, 1491–1499.

(21) Chesnavich, W. J. *J. Chem. Phys.* **1986**, *84*, 2615–2619.

(22) Hase, W. L. *J. Chem. Phys.* **1976**, *64*, 2442–2449.

(23) Quack, M.; Troe, J. *Ber. Bunsenges. Phys. Chem.* **1974**, *78*, 240–252.

(24) Troe, J. *J. Chem. Phys.* **1987**, *87*, 2773–2780.

(25) Troe, J. *J. Chem. Soc., Faraday Trans.* **1997**, *93* (5), 885–891.

(26) Chesnavich, W. J.; Bowers, M. T. *J. Chem. Phys.* **1977**, *66*, 2306–2315.

(27) Dyson, F. *Nature* **2004**, *427*, 297.

(28) Morrow, J. C.; Baer, T. *J. Phys. Chem.* **1988**, *92*, 6567–6571.

(29) Ketvirtis, A. E.; Baranov, Y. I.; Hopkinson, A. C.; Bohme, D. K. *J. Phys. Chem. A* **1998**, *102* (7), 1162–1169.

(30) Zaluzhna, O.; Simmons, J. G.; Heard, G. L.; Setser, D. W.; Holmes, B. E. *J. Phys. Chem. A* **2008**, *112* (27), 6090–6097.

(31) Weber, M. E.; Armentrout, P. B. *J. Phys. Chem.* **1989**, *93* (4), 1596–1604.

(32) Bauschlicher, C. W.; Partridge, H. *Chem. Phys. Lett.* **1997**, *276* (1−2), 47–54.

(33) Karton, A.; Martin, J. M. L. *J. Phys. Chem. A* **2007**, *111*, 5936–5944.

(34) Bodi, A.; Kercher, J. P.; Bond, C.; Meteesatien, P.; Sztáray, B.; Baer, T. *J. Phys. Chem. A* **2006**, *110*, 13425–13433.

(35) Ruscic, B.; Boggs, J. E.; Burcat, A.; Császár, A. G.; Demaison, J.; Janoschek, R.; Martin, J. M. L.; Morton, M. L.; Rossi, M. J.; Stanton, J. F.; Szalay, P. G.; Westmoreland, P. R.; Zabel, F.; Berces, T. *J. Phys. Chem. Ref. Data* **2005**, *34*, 573–656.

(36) Lazarou, Y. G.; Papadimitriou, V. C.; Vassileios, C.; Prosmitis, A. V.; Papagiannakopoulos, P. *J. Phys. Chem. A* **2002**, *106*, 11502–11517.

(37) DeMore, W. B.; Sander, S. P.; Golden, D. M.; Hampson, R. F.; Kurylo, M. J.; Howard, C. J.; Ravishankara, A. R.; Kolb, C. E.; Molina, M. J. *Chemical kinetics and photochemistry data for use in stratospheric modelling*; 97−4; JPL publication, 97.

(38) Parthiban, S.; Martin, J. M. L. *J. Chem. Phys.* **2001**, *114*, 6014–6029.

(39) Kaiser, E. W.; Wallington, T. J. *J. Phys. Chem.* **1996**, *100*, 411–419.

(40) Becerra, R.; Walsh, R. In *The Chemistry of Organic Silicon Compounds*; Rappoport, Z., Apoeloig, Y., Eds.; John Wiley & Sons: New York, 1998.

(41) Hildenbrand, D. L.; Lau, K. H.; Sanjurjo, A. *J. Phys. Chem. A* **2003**, *107* (28), 5448–5451.

(42) Walsh, R. Thermochemistry. In *The Chemistry of Organic Silicon Compounds*; Patai, S., Rappoport, Z., Eds.; John Wiley & Sons: New York, 1989; pp 371−391.